International Conference on Computational Methods in Marine Engineering
MARINE 2011
L.Eça, E. Oñate, J. García, T. Kvamsdal and P. Bergan (Eds)

LARGE EDDY SIMULATION OF THE FLOW PAST THE DTMB5415 SURFACE COMBATANT HULL WITH AND WITHOUT BILGE KEELS

Urban Svennberg*, Christer Fureby*†, Mattias Liefvendahl* and Niklas Alin*

*Swedish Defence Research Agency - FOI, SE 147 25 Tumba, Stockholm, Sweden e-mail: mattias.liefvendahl@foi.se, www.foi.se

†Dept. of Shipping and Marine Technology, Chalmers University of Technology, SE-412 96, Gothenburg, Sweden

Key words: Large Eddy Simulation (LES), Naval Hydrodynamics

Abstract. The flow around the DTMB5415 surface combatant hull with and without bilge keels is studied numerically by the use of a Large Eddy Simulation (LES) method. The main purpose for bilge keels is to reduce roll motions when operating in ocean waves. The flow resistance should at the same time be affected as little as possible. The computations presented here are for straight course in calm water conditions and show only a small change in the wake of the hull and there by a minimal effect on the resistance. The computations are made as a preparatory step before investigating other conditions, such as yaw angle.

1 INTRODUCTION

Generally, there is a strong interest in developing improved and optimized ships. The design objectives can be very different depending on the purpose of the ship. It can be the need for increased load capacity achieved by a more lightweight constructions that at the same time is stronger, the need for lower fuel consumption from economical and environmental points of view, and the need for hydrodynamically more efficient hulls and propulsion systems. For naval ships the main motivation is to reduce signatures and thus to reduce the vulnerability of the ship. Detailed knowledge about the hydrodynamic flow around the hull is therefore essential to achieve many of the desired improvements.

The flow past a surface ship hull is complicated due to the flow features induced by the shape of the hull, including developing boundary layers, vortex structures from appendages, such as bilge keels, sonar domes, struts and shafts, high Reynolds (Re) number turbulence and the free water surface. In the past, potential flow methods,[1] proved useful in predicting the gross features of the flow including the pressure distributions and

wave-pattern, but more recently these methods have started to be replaced by Reynolds Averaged Navier-Stokes (RANS) models,[2,3] which have the ability to predict the mean pressure, velocity and free-surface distributions around the hull together with estimates of the turbulence. RANS can give acceptable predictions of drag and mean velocities but towards the stern, where the flow becomes extremely complicated, RANS is not always able to predict the mean flow, and certainly not the unsteady coherent flow structures. More advanced Computational Fluid Dynamics (CFD) models such as Detached Eddy Simulation (DES),[4,5] and LES,[5,6] have the ability to predict the unsteady coherent vortex structure dynamics. Only a few DES and LES type computations of surface ship hydrodynamics have so far been presented in the open literature,[4–9] but these results indicate that the DES/LES approaches have the capability to capture essential features that RANS cannot capture.

The study described here is a continuation of previous work,[6,7] which here is extended by a computation with bilge keels. We aim at investigating the predictive capabilities of LES,[10–13] for surface ship hydrodynamics by computing and comparing the unsteady flow past the DTMB5415 surface combatant hull with and without bilge keels.

2 MATHEMETICAL FORMULATION OF FREE SURFACE LES

The flow physics involved in surface ship hydrodynamics consists primarily of high Re-number boundary layer dominated incompressible flow around the hull, the generation and evolution of the surface wave pattern, and the wake stretching far astern of the ship. The governing equations are the incompressible Navier Stokes Equations,[14] modeling the flow of air and water, and an additional equation for the evolution of the interface between these two immiscible fluids. Different approaches can be used for tracking the air-water interface,[15] and here we use the Volume of Fluids (VoF) approach,[15,16] in which a volume fraction, α, taking the value 0 in air, 1 in water and $0 < \alpha < 1$ in regions where the two fluids co-exists, is employed to represent the air-water interface. The governing equations are thus,

$$\begin{cases} \partial_t(\rho\mathbf{v}) + \nabla\cdot(\rho\mathbf{v}\otimes\mathbf{v}) = -\nabla p + \nabla\cdot\mathbf{S} + \rho\mathbf{f} \\ \nabla\cdot\mathbf{v} = 0 \\ \partial_t(\alpha) + \nabla\cdot(\alpha\mathbf{v}) = 0 \end{cases} \tag{1}$$

where $\mathbf{v}$ is the velocity, ρ the density, p the pressure, $\mathbf{S} = 2\mu\mathbf{D}$ the viscous stress tensor, $\mu = \alpha\mu_1 + (1-\alpha)\mu_2$ the viscosity, $\mathbf{D} = 1/2(\nabla\mathbf{v} + \nabla\mathbf{v}^T)$ the rate-of-strain tensor, $\nabla\mathbf{v}$ the velocity gradient, and $\mathbf{f}$ the specific body force consisting of the gravitational acceleration and surface tension. In the above expressions indices 1 and 2 refers to the water and the air phase, respectively, whereas for free-surface ship hydrodynamics the surface tension is neglected.

The motivation behind LES was to establish a simulation framework that properly resolves the coherent structure dynamics, modeling the residual flow in a manner consistent

with the cascade process,[17] and thus being more accurate than RANS and less expensive than DNS. For LES to work as intended the coherent structure dynamics must be resolved on the grid together with the large-scale part of the energy cascade, necessitating carefully designed grids with good resolution in regions of coherent structure activity. The equations governing the large-scale flow features are then obtained by applying a spatial filter, having a width of Δ, to (1) in order to eliminate the small-scale flow features. After spatial filtering and rearranging of terms, the governing equations for the large (resolved) eddy scales becomes,

$$\begin{cases} \partial_t(\rho\overline{\mathbf{v}}) + \nabla\cdot(\rho\overline{\mathbf{v}}\otimes\overline{\mathbf{v}}) = -\nabla\overline{p} + \nabla\cdot(\overline{\mathbf{S}} - \mathbf{B}) + \rho\overline{\mathbf{f}} \\ \nabla\cdot\overline{\mathbf{v}} = 0 \\ \partial_t(\overline{\alpha}) + \nabla\cdot(\overline{\alpha}\overline{\mathbf{v}}) = -\nabla\cdot\mathbf{b} \end{cases} \tag{2}$$

where overbars denote spatially filtered variables, $\mathbf{B} = \rho(\overline{\mathbf{v}\otimes\mathbf{v}} - \overline{\mathbf{v}}\otimes\overline{\mathbf{v}})$ the subgrid stress tensor and $\mathbf{b} = \overline{\alpha\,\mathbf{v}} - \overline{\alpha}\,\overline{\mathbf{v}}$ the subgrid flux vector which both must be modeled in order to close (2). The demands on the sub-grid models are expected to be less severe compared to RANS since a substantial fraction of the coherent structure dynamics is resolved. However, as the hull is approached, the flow structures change character, and the flow becomes dominated by longitudinal vortices with a characteristic length and spacing, which form Ω-shaped vortex structures that interacts with the bulk flow. The scales dominating the near wall flow varies with the Re-number, and are much smaller than those of the detached or free flow, requiring either grid refinement as the wall is approached, or the use of a LES wall model.

The subgrid stress tensor $\mathbf{B}$ and subgrid flux vector $\mathbf{b}$ are here both modeled by structural models,[10] designed to retain as much as possible of the physics embedded in these terms, but at the expense of some numerical stability that may lead to ripples in e.g. the computed free surface wave field. We here use a One Equation Eddy Viscosity Model (OEEVM) that is composed of a subgrid viscosity term, $-2\rho\nu_k\overline{\mathbf{D}}$, representing the subgrid dissipation. The model then consists of $\mathbf{B} \approx -2\rho\nu_k\overline{\mathbf{D}}$ and $\mathbf{b} \approx -\nu_k\nabla\overline{\alpha}$, in which the subgrid viscosity, ν_k, is estimated as $\nu_k = c_k\Delta k^{1/2}$, in which the subgrid kinetic energy, k, is assumed to evolve according to the following (modeled) transport equation,[18]

$$\partial_t(k) + \nabla\cdot(k\overline{\mathbf{v}}) = 2\nu_k\left\|\overline{\mathbf{D}}\right\|^2 + \nabla\cdot(\nu_k\nabla k) - c_\epsilon k^{2/3}/\Delta \tag{3}$$

where $\epsilon = c_\epsilon k^{2/3}/\Delta$ is the subgrid dissipation.[10] The model coefficients $c_k = 0.07$ and $c_\epsilon = 1.03$ are obtained from an expected inertial sub-range behavior. To alleviate the extreme resolution requirements close to the hull the subgrid model is adjusted as the hull is approached. More precisely, adjacent to the hull the total viscosity, $\nu + \nu_k$, is replaced by $\tau_w/(\partial v_v/\partial y)|_w$, in which τ_w has been computed from an assumed log-law behavior of the velocity.

3 NUMERICAL METHODS

The governing equations (2) and (3) are here discretized using an unstructured collocated Finite Volume (FV) method based on the OpenFoam C++ library.[19] The dependent variables are represented by control volume averages $f_p = \frac{1}{\delta V_p}\int_{\Omega_p} f(\mathbf{x},t)\mathrm{dV}$, formally defining the spatial filtering in (2), and by using Reynolds transport theorem together with a multi-step time integration procedure the LES equations (2) can be discretized, resulting in,

$$\begin{cases} \dfrac{\beta_i \Delta t}{\delta V_P}\Sigma_f \left[F_f^{C,\rho}\right]^{n+i} = 0 \\ \Sigma_{i=0}^{m}(\alpha_i(\overline{\rho}\,\overline{\mathbf{v}})_P^{n+i} + \dfrac{\beta_i \Delta t}{\delta V_P}\Sigma_f \left[F_f^{C,v} + F_f^{D,v} + F_f^{B,v}\right]^{n+i}) = \beta_i(\nabla\overline{p})_P^{n+i}\Delta t + \beta_i(\overline{\mathbf{f}})_i^{n+i}\Delta t \\ \Sigma_{i=0}^{m}(\alpha_i(\alpha)_P^{n+i} + \dfrac{\beta_i \Delta t}{\delta V_P}\Sigma_f \left[F_f^{C,\alpha}\right]^{n+i}) = 0 \end{cases} \quad (4)$$

where α_i and β_i are parameters of the multi-step time-integration scheme whereas $F_f^{C,\rho} = (\overline{\mathbf{v}}\mathrm{dA})_f$, $F_f^{C,v} = (\overline{\mathbf{v}}\mathrm{dA})_f\mathbf{v}_f$, $F_f^{D,v} = (\nu\nabla\overline{\mathbf{v}})_f\mathrm{dA}$, $F_f^{C,\alpha} = (\overline{\mathbf{v}}\mathrm{dA})_f\overline{\alpha}_f$, $F_f^{B,v} = (\mathbf{B})_f\mathrm{dA}$ and $F_f^{b,\alpha} = (\mathbf{b})_f\mathrm{dA}$ are the fluxes across the cell face with index f. To close the FV-discretization the fluxes need to be reconstructed from the variables at neighboring cells. Linear interpolation is used for the convective terms in the momentum equation and linear approximations are used to evaluate the inner derivatives in the viscous and subgrid fluxes. For the momentum equation this results in second order accurate schemes, respectively, whereas a specific treatment is used to handle the reconstruction of the fluxes in the α-equation, since the interface is required to be as sharp as possible. The pressure velocity system is here decoupled by combining (4_1) and (4_2) into a Poisson equation for $\overline{p}$ that is solved together with (4_2) and (4_3) using a PISO (Pressure Implicit with Splitting of Operators) algorithm with a modified Rhie and Chow interpolation for cell-centered data.[20] The equations are solved sequentially with iteration over the coupling terms to obtain rapid convergence. The convective fluxes of the α-equation (4_3) are reconstructed using a novel flux reconstruction formulation,

$$F_f^{C,\alpha} \approx \left[F_f^{C,\rho}\alpha_f^{R1} + \left|F_f^{C,\rho}\right| / \left|\mathrm{dA}_f\right| \mathbf{n}(1-\alpha_f^{R2})\alpha_f^{R2}\right],$$

in which $\mathbf{n}$ is the unit normal vector to α, and the superscripts $R1$ and $R2$ denotes two different flux reconstruction algorithms. For the simulations presented here the two flux reconstruction schemes $R1$ and $R2$ are chosen to be the conventional bounded linear scheme and the van-Leer scheme, respectively.

4 THE HULL MODEL

The model hull under consideration is the surface combatant DTMB5415[21–24] (also denoted INSEAN2340 model). The flow around two configurations have been simulated,

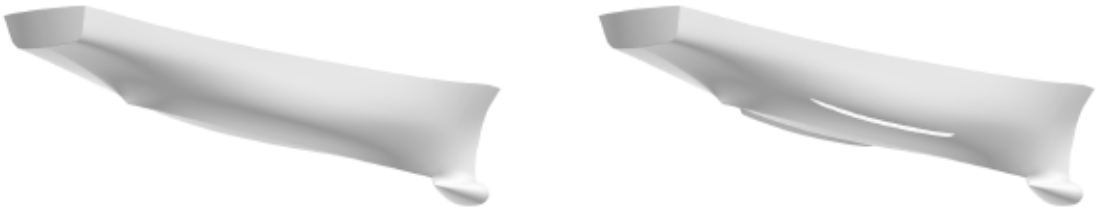

(a) (b)

Figure 1: DTMB5415 surface combatant model. Without bilge keels (a) and with bilge keels (b).

with and without bilge keels, as shown in Figure 1. A unique aspect of this hull is that it has been used in a collaborative effort between David Taylor Model Basin, Iowa Institute of Hydraulic Research, and the Italian Ship Model Basin in order to obtain a complete data set at various conditions and to provide information on facility biases as there were repeated runs between the facilities.[24] Here, the hull, with a length of L=5.72 m, is sunk and trimmed by amounts given from the experiment and was run straight ahead at a speed of 4.2 knots (2.165 m/s) giving a Re-number of $12 \cdot 10^6$, based on L, and a Fr-number of 0.289.

The computational domain has an overall length of 3.4L and an overall width of 4.2L, including the external sponge region of width L, with the hull positioned at y=0, with the forward perpendicular at x/L=0.5 downstream of the inlet plane. The height of the computational domain is 0.7L, with the nominal free water surface being located 0.5L above the lower computational boundary. Representative physical values for densities and viscosities are selected for water and air.

Both computations are performed using the same subgrid model, the OEEVM with wall model and VoF. Two multi-block structured grids have been generated, with $6.6 \cdot 10^6$ and $8.6 \cdot 10^6$ hexahedral control volumes respectively. The finer grid has the same topological structure as the coarser but have a general longitudinal refinement along the bilge keels and refinement around the bilge keels to better resolve their geometry. A grid refinement test in order to analyze the sensitivity of the LES predictions to the grid size has been performed and show that the grid resolution is sufficient to capture the main flow structures accurately.[7] The velocity and undisturbed free surface location are prescribed on the inflow plane, and at the outflow Neumann conditions are used for all quantities except the pressure, which is set to a constant value. On the hull, no-slip conditions are used, as facilitated by the use of subgrid wall models. A uniform velocity, a constant pressure and the domain divided into air and water through the α-field serves as initial conditions.

5 RESULTS

The flow around the underwater part of the hull is dominated by the vortices generated by the sonar dome, the developing boundary layer and the interaction between the vortices and the boundary layer. Figure 2 presents the flow beneath the hull in terms of vortical

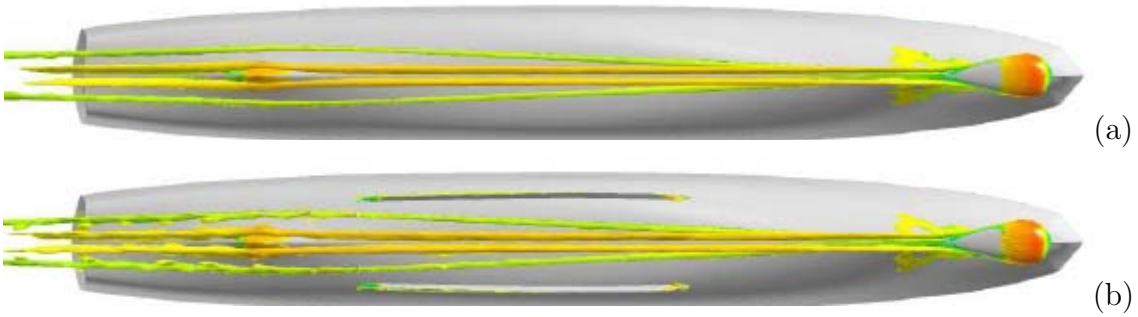

Figure 2: Instantaneous flow structures beneath the hull illustrated by an iso-surface of the second invariant of the velocity gradient, colored by the local axial velocity. (a) Without bilge keels and (b) with bilge keels.

structures, represented by iso-surfaces of the second invariant of the velocity gradient. The flow at the bow has a large downward component on each side of the bow, growing in size and strength as it is advected downstream whilst interacting with the hull boundary layer. At the edge of the sonar dome this results in a counter-rotating bow dome vortex pair detaching from the trailing tip of the sonar dome, and becomes enhanced by the inward and downward flow over the forward bilge after which it continues downstream beneath the hull close to the keel at some distance from the hull. Furthermore, the flow over the upper part of the sonar dome and lower part of the bow roll-up and form a strong vortex on each side of the keel, the so-called bilge vortex, that is partially located within the hull boundary layer and further away from the keel. While the sonar dome vortex pair is relatively stable, the bilge vortex system is unsteady as it interacts with the evolving hull boundary layer, resulting in new vortical structures, whilst being advected downstream. Towards the transom stern, the hull boundary layer thickens, and the bilge vortex system partly detaches from the hull boundary layer and becoming rounder and weaker, as well as giving birth to multiple vortices. The sonar dome vortex pair is less affected by the pressure difference caused by the transom stern and is therefore also less deflected vertically. The bow of the hull is modified well above the waterline to avoid severe skewness in some cells in the computational grid and thereby increase the quality in it. This modification only affect the airflow and not the waves and the motion of the water. The bilge keels are not perfectly aligned with the flow for straight course at this Fr-number. Therefore, there are small vortical structures generated by the bilge keels. This also results in a small change in the crossflow underneath the hull as well, not strong enough however to give any visible alteration of the location of the vortices from the sonar dome, but it appears to be sufficient to affect the stability of these vortices, see Figure 2b.

The normalized time averaged axial velocity around the bilge keel is shown at four cross-sections, x/L=0.4, x/L=0.5, x/L=0.6 and x/L=0.7 respectively, in Figure 3. Figure 3c, at x/L=0.6, shows that there is some crossflow outwards over the bilge keel generating a small vortex at the tip of the keel. This vortex and the boundary layer from the bilge

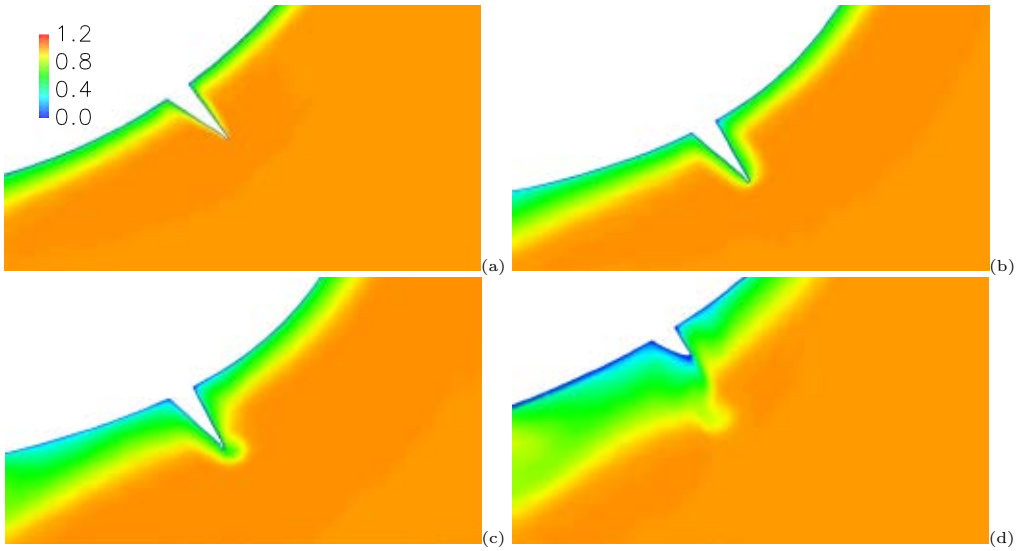

Figure 3: Contours of the normalized time averaged axial velocity around the bilge keel. (a) at x/L=0.4, (b) at x/L=0.5, (c) at x/L=0.6 and (d) at x/L=0.7.

keel leave an imprint on the boundary layer of the hull, see Figure 3d, at the end of the keel at x/L=0.7.

Figure 4 shows the time averaged axial velocity underneath the hull in seven cross-planes, x/L=0.2, x/L=0.4, x/L=0.6, x/L=0.8, x/L=0.9346 x/L=1.0 and x/L=1.1 respectively, for the experimental data,[21] and the computations with and without bilge keels. There are two experimental figures at the first station, x/L=0.2, Figure 4.1a, where a small patch at the sonar dome vortex has been measured with higher resolution, showing that the experimental data for the other cross-sections can miss some details that are resolved in the computations. There are no visible differences between the computations at the first station, Figures 4.1b and 4.1c, which is expected since this station is well upstream of the bilge keels. There as a noticeable acceleration of the axial flow just outside of the keels, more on the inside than on the outside of them, at the second station, x/L=0.4, Figures 4.2b and 4.2c. This effect is stronger at the third station, at x/L=0.6, Figures 4.3b and 4.3c, where the boundary layer also is slightly thicker under the hull inside of the bilge keels, which is a result of the fact that the bilge keels are not perfectly aligned with the flow for this combination of Fr- and Re-numbers. This results in a somewhat more “compressed” flow between the bilge keels than in the case without bilge keels. The flow field will have somewhat different form for different velocities which makes the alignment of the bilge keels perfectly good only for the velocity that they are optimized for. The most noticeable feature at stations 4-7 is a small extra “hump” on the outside of the wake from the sonar dome vortices, Figure 4. The main purpose of the bilge keels is to reduce roll motions without a noticeable effect on the resistance of the hull. It is therefore natural that the effect on the wake is very small for a steady velocity

at a straight course. On the other hand, for a yaw angel or roll motion, there will be a strong crossflow over the bilge keels resulting in separation and generation of vortices, a process that will draw energy from the crossflow and thereby damping the roll motion or increase the resistance for a yaw motion.

The computed flow without bilge keels is generally in very good agreement with the experimental data at all cross-sections, thus capturing the development of the boundary layer and the vortices from the sonar dome and the hull.

The normalized turbulent kinetic energy is shown in Figure 5, experimental data is shown in Figure 5a, the total turbulent kinetic energy from the computations is shown i Figure 5b and 5c and the unresolved part of the turbulent kinetic energy computed by the subgrid model is shown in Figure 5d and 5e. The experimental data for the turbulent kinetic energy are taken from measurements on a smaller model,[22] thus the Re-number in the experiment is $5 \cdot 10^6$ here while it is $12 \cdot 10^6$ in the computations and in the velocity data presented above. The majority of the subgrid energy is found close to the hull and in the vortex structures close to the hull close to the centerline. The subgrid energy is somewhat more concentrated than the experimental data but at the same levels in this structure. The outer part of the vortical structures under the hull only have a very small amount of subgrid energy but the flow structures here are sufficiently resolved to get the correct amount of turbulent kinetic energy in the resolved part of the flow field, see Figures 5b and 5c. The resolved turbulent kinetic energy have high values in the vortical structure close to the hull. The energy here is mainly found in axial velocity fluctuations resulting in a maximum local turbulent energy approximately three times higher than in the experiments. The are some possible explanations for this difference between the experiments and the computations, relating to the difference in Re-number, to measurement accuracy and to numerical and modeling issues. The difference in Re-number is relatively small and should only give small differences in the velocity field, including its the fluctuations. The experiments are conducted using Particle Image Velocimetry (PIV)[22] which is a method that gives a very good overview of the flow field and the dimensions of vortex and turbulent structures but it is not as accurate as Laser Doppler Velocimetry (LDV) concerning the velocity components. The turbulent velocity fluctuations are about 5% of the free-stream velocity in the experiments and about 10% in the computations, which both can be considered as reasonable levels for the turbulent flow around a ship hull. These small values, relative to the free-stream velocity, make it challenging tasks both to measure the turbulent kinetic energy accurately and to compute it. Numerical issues, such as stabilty problems, can give exaggerated levels of fluctuations, but a careful investigation of the computed flow field does not give any indications of stability problems. Furthermore, a too high level of turbulent fluctuations should increase the turbulent difusion of the vortices reducing their strength and the turbulence here does not appear to have a negative effect on the computation of the vortex strength and the flow field. Bhushan et al only obtain 25% of the experimental levels of turbulent fluctuations in their DES computation,[9] which results in stronger and

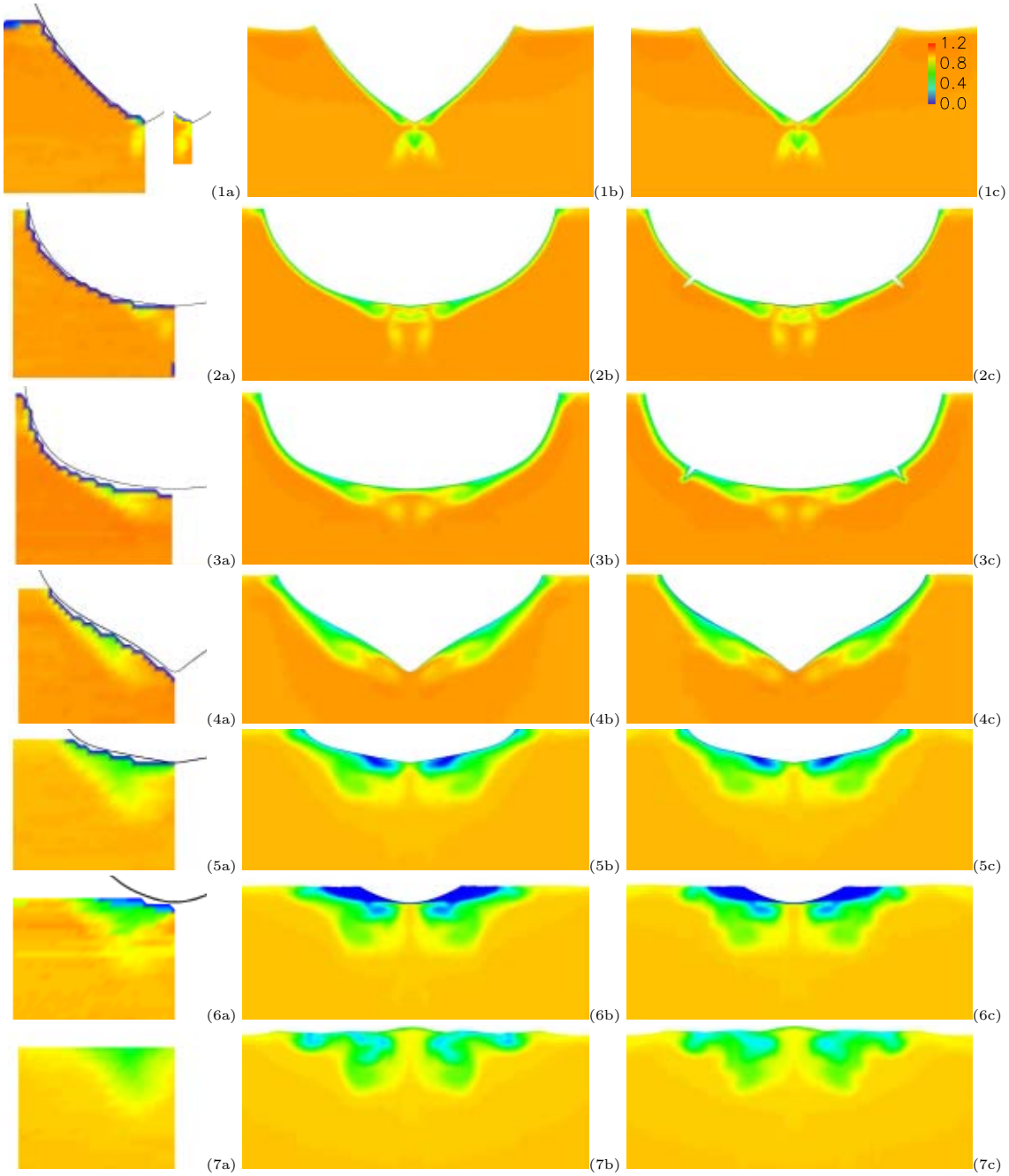

Figure 4: Contours of the normalized time averaged axial velocity. Column (a) experimental data, (b) without bilge keels and (c) with bilge keels. Row (1) at x/L=0.2, (2) at x/L=0.4, (3) at x/L=0.6, (4) at x/L=0.8, (5) at x/L=0.9346, (6) at x/L=1.0 and (7) at x/L=1.1.

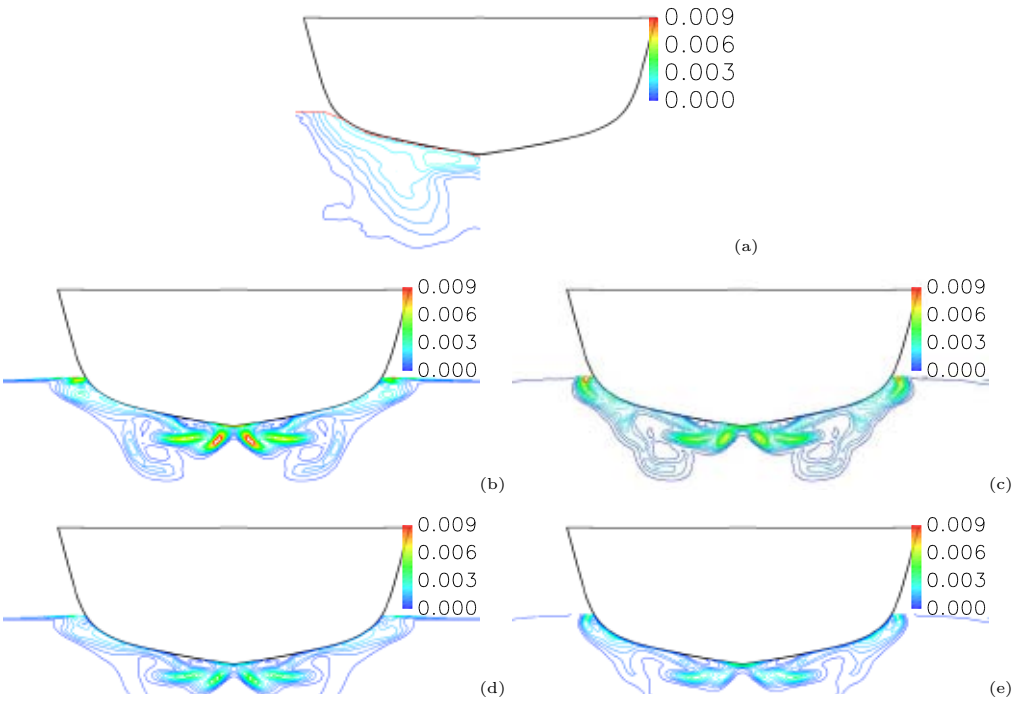

Figure 5: Contours of the normalized time averaged turbulent kinetic energy, at $x/L = 0.9346$. Experimental data (a), LES without bilge keels (b), LES with bilge keels (c), the unresolved turbulent kinetic energy in LES without bilge keels (d), and the unresolved turbulent kinetik energy in LES with bilge keels (e).

more concentrated vortices than in the experiments.

The wakes from the bilge keels redistribute the turbulent energy in the outer part of the wake which can be seen by comparing Figures 5b and 5c. There are also small differences in the shape of the unresolved subgrid turbulent wake between the two configurations, as can be seen in Figures 5d and 5e.

6 CONCLUDING REMARKS

Computations of the flow around the DTMB5415 surface combatant, with and without bilge keels, have been conducted and compared to each other and to experimental data without bilge keels. The computational results without bilge keels are in close agreement with the experimental data for the velocity components at all cross-sections. However, the turbulent kinetic energy is exaggerated in the computations, locally around the vortices from the sonar dome close to the hull at the propeller plane cross-section. The velocity components appear to be unaffected by this local overprediction.

The computations were carried out for calm sea condition for a steady course straight ahead as a preparatory step for further computations in other operating conditions. Only small modifications in the flow, generated by the bilge keels, are expected if the bilge

keels are aligned with the local flow. The computations confirm that the bilge keels are almost perfectly aligned with the flow and that the differences between the flow field with and without bilge keels are small, but detectable. This shows that the grid and the computational model are sufficiently accurate for us to proceed to the more advanced computations with a yaw angle and bilge keels.

REFERENCES

[1] Larsson L. and Baba E. Ship resistance and flow computations. In *Advances in Marine Hydrodynamics*, Boston, USA, 1996.

[2] Wilcox D.C. *Turbulence Modelling for CFD.* DCW Industries, 1998.

[3] Paterson E., Hyman M., Stern F., Bonetto F., Drew D., and Lahey R. Near and Farfield CFD for a Naval Combatant including Thermal Stratification and Two-fluid Modeling. In *21st Symp. on Naval Hydrodynamics*, Trondheim, Norway, 1996.

[4] Nikitin N.V., Nicoud F., Wasistho B., Squires K.D., and Spalart P.R. An Approach to Wall Modeling in Large Eddy Simulation. *Phys. Fluids*, 2000.

[5] Yang J., Bhushan S., Suh J.S., Wang Z., Koo B., Sakamoto N., Xing T., and Stern F. Large Eddy Simulation of Ship Flows with Wall Layer Models on Cartesian Grids. In *27st Symp. on Naval Hydrodynamics*, Seoul, Korea, 2008.

[6] Alin N., Fureby C., Parmhed O., and Svennberg U. Large Eddy Simulation of the flow past the DTMB5415 hull. In *27st Symp. on Naval Hydrodynamics*, Seoul, Korea, 2008.

[7] C. Fureby, N. Alin, and M. Liefvendahl. Large Eddy Simulation of the flow past the DTMB5415 surface combatant hull. In *Gothenburg 2010 A Workshop on Numerical Ship Hydrodynamics*, number R-10:122, Chalmers University of Technology, Gothenburg, Sweden, 2010.

[8] Xing T., Carrica P., and Stern F. Large-Scale RANS and DDES Computations of KVLCC2 at Drift Angle 0 Degree. In *Gothenburg 2010 A Workshop on Numerical Ship Hydrodynamics*, Chalmers University of Technology, Gothenburg, Sweden, 2010.

[9] Bhushan S., Michael T., Yang J., Carrica P., and Stern F. Fixed Sinkage and Trim Bare Hull 5415 Simulations using CFDSHIP-IOWA. In *Gothenburg 2010 A Workshop on Numerical Ship Hydrodynamics*, Chalmers University of Technology, Gothenburg, Sweden, 2010.

[10] Sagaut P. *Large Eddy Simulation for Incompressible Flows.* Springer Verlag, 2001.

[11] Grinstein F.F., Margolin L., and Rider B. *Implicit Large Eddy Simulation: Computing Turbulent Fluid Dynamics.* Cambridge University Press, 2007.

[12] Fureby C. Towards Large Eddy Simulation in Engineering. *Prog. Aerospace Science*, 2008.

[13] C. Fureby. Large Eddy Simulation of Ship Hydrodynamics. In *27th Symp. on Naval Hydrodynamics*, Seoul, Korea, 2008.

[14] Gurtin M. E. *An Introduction to Continuum Mechanics*. Academic Press, 1981.

[15] Ubbink O. *Numerical Prediction of Two Fluid Systems with Sharp Interfaces*. PhD thesis, London University, 1997.

[16] Hirt C.W. and Nichols B.D. Volume of Fluid (VOF) Method for the Dynamics of Free Boundaries. *Journal of Computational Physics*, 1981.

[17] Pope S. B. *Turbulent Flows*. Cambridge University Press, 2000.

[18] Bensow R. and Fureby C. On the Justification and Extension of Mixed Models in LES. *Journal of Turbulence*, 2007.

[19] Weller H.G., Tabor G., Jasak H., and Fureby C. A Tensorial Approach to CFD using Object Oriented Techniques. *Comp. in Physics*, 1997.

[20] Issa R. I. Solution of the implicitly discretized fluid flow equations by operator splitting. *J. Comp. Physics*, 1986.

[21] Olivieri A., Pistani F., Avanzini A., Stern F., , and R. Penna. Towing Tank Experiments of Resistance, Sinkage and Trim, Boundary Layer, Wake, and Free Surface Flow Around a Naval Combatant INSEAN 2340 Model. Technical Report IIHR Report No. 421, Iowa Institute of Hydraulic Research, University of Iowa, USA, 2001.

[22] Longo J., Shao J., Irvine M., and Stern F. Phase-Averaged PIV for the Nominal Wake of a Surface Ship in Head Waves. *J. Fluids Eng.*, 2007.

[23] Larsson L., Stern F., and Bertram V. Benchmarking of Computational Fluid Dynamics for Ship Flows: The Gothenburg 2000 Workshop. *J. Ship Res.*, 2003.

[24] Stern F., Longo J., Penna R., Olivieri A., and Ratcliffe T. International Collaboration on Benchmark CFD Validation Data for Surface Combatant DTMB Model 5415. In *23st Symp. on Naval Hydrodynamics*, Val de Reuil, France, 2000.